Conserved sites on the influenza H1 and H3 hemagglutinin recognized by human antibodies

Daniel P. Maurer[1], Mya Vu[1*], Ana Sofia Ferreira Ramos[3*], Haley L. Dugan[4*], Paul Khalife[4*], James C. Geoghegan[4], Laura M. Walker[5], Goran Bajic[3], Aaron G. Schmidt[1,2]

[1]Ragon Institute of Mass General, MIT, and Harvard, Cambridge, MA, 02139, USA

[2]Department of Microbiology, Harvard Medical School, Boston, MA 02115, USA

[3]Department of Microbiology, Icahn School of Medicine at Mount Sinai, New York, NY 10029, USA

[4]Adimab, LLC, Lebanon, NH 03766, USA

[5]Invivyd Inc., Waltham, MA 02451, USA

[*]These authors contributed equally

Key words: influenza, antibodies, viral escape

Correspondence:
Aaron G. Schmidt
E-mail: aschmidt@crystal.harvard.edu

ABSTRACT

Monoclonal antibodies (mAbs) targeting the influenza hemagglutinin (HA) have the potential to be used as prophylactics or templates for next-generation vaccines that provide broad protection. Here, we isolated broad, subtype-neutralizing mAbs from human B cells targeting the H1 or H3 HA head as well as a unique mAb targeting the stem. The H1 mAbs target the previously defined lateral patch epitope on H1 HAs and recognize HAs from 1933 to 2021 in addition to a swine H1N1 virus with pandemic potential. Using directed evolution, we improved the neutralization potency of these H1 mAbs towards a contemporary H1 strain. Using deep mutational scanning of four antigenically distinct H1N1 viruses, we identified potential viral escape pathways. For the H3 mAbs we used cryo-EM to define the targeted epitopes: one mAb recognizes the side of the H3 head, accommodating the N133 glycan and a pocket underneath the receptor binding site. The other H3 mAb recognizes an epitope in the HA stem that overlaps with previously characterized mAbs, but with distinct antibody variable genes and mode of recognition. Collectively, these mAbs identify common sites recognized by broad, subtype-specific mAbs that may be elicited by next-generation vaccines.

INTRODUCTION

Two influenza types cause human disease: influenza A viruses (IAVs) emerge from animal reservoirs and cause global pandemics while influenza B viruses (IBVs) only circulate in the human population. Antigenic and genetic differences of the major surface glycoprotein hemagglutinin (HA), which engages the sialic acid receptor and fuses the viral and endosomal membranes, further divide IAVs into two groups with 18 HA subtypes (H1–H18) total. In the last century, IAVs bearing H1 or H2 (group 1), or H3 (group 2) HAs have circulated in the human population; H1N1 and H3N2 viruses currently circulate.

Vaccine effectiveness against seasonal influenza viruses reaches modest levels around 50%[1] and updated vaccines are needed due to antigenic drift – the acquisition of amino acid mutations in HA that preserve function but escape population-wide antibody recognition. IAVs undergo antigenic drift more rapidly than IBVs[2], requiring continuous monitoring for new antigenic variants. Additional barriers to an effective vaccine include complex and variable immune histories within the human population. A complementary approach to seasonal vaccination is to identify monoclonal antibodies (mAbs) that recognize conserved HA sites for prophylactic use, particularly in high-risk populations. Characterizing such mAbs can also serve as templates to guide next-generation vaccine designs and inform how viral escape from vaccine-induced immunity may occur.

Antibodies that target the HA "head" and prevent sialic acid receptor engagement are an established correlate of protection but are usually subtype-specific[3-5]. mAbs with heterosubtypic breadth typically engage epitopes on the membrane proximal HA "stem" within group 1 or group 2, and, in some cases, both[6-10]. Although these stem-directed mAbs are protective in mice[6-10], they require Fc-effector functions for protection, suggesting that although stem-directed mAbs can neutralize *in vitro*, there is minimal neutralization activity *in vivo*[11]. Due to their reactivity to potentially pandemic subtypes of IAVs that have not circulated in humans, stem-directed mAbs may help protect from severe disease in the case of zoonotic spillover or viral escape from anti-head mAbs. However, while passive transfer of stem-directed antibodies offers some protection, head-directed antibodies better protect against acquiring infection even when normalized by binding titers[12].

In contrast to anti-stem mAbs, IAVs escape anti-head antibodies frequently at the population level, demonstrating that these mAbs provide a significant barrier for transmission that

75 the virus must overcome to persist in the population[2,13,14]. Although epitopes in the head are more
76 variable than the stem, it is nevertheless possible to identify broad, subtype-specific anti-head
77 mAbs[15-24]. Epitopes on the side of the HA head (*e.g.,* the lateral patch, vestigial esterase) are
78 conserved[15,21,22], affording mAbs targeting these sites considerable breadth and potency. If next-
79 generation vaccines can elicit antibodies targeting these conserved epitopes[25-27], it is unclear how
80 such a diverse polyclonal response would structurally recognize HA and ultimately how the virus
81 would evolve to escape.

82 Here, we isolated and characterized broad H1 and H3 human mAbs capable of neutralizing
83 human IAVs spanning several decades. For the broad H1 mAbs, which neutralize H1N1 IAVs
84 spanning ~100 years, we used four deep mutational scanning H1N1 viral libraries to map critical
85 residues within the targeted epitope. Although escape from broad H1 mAbs was readily selected
86 *in vitro*, human influenza H1N1 isolates have rarely contained these escape mutations. Broad H1
87 mAb neutralizing potency was improved against a contemporary H1N1 strain using directed
88 evolution. For the broad H3 mAbs, which neutralize human H3N2 IAVs spanning ~50 years, we
89 determined cryo-EM structures in complex with HA. One broad H3 mAb targets an epitope in the
90 head domain with regions of low mutational tolerance[28]. The other broad H3 mAb targets the group
91 2 stem site but engages with a distinct mode of recognition. The epitopes identified by these broad
92 H3 mAbs overlap with those targeted by previously characterized mAbs, but with different
93 antibody variable gene usage and paratopes. These data suggest that while antibodies targeting
94 these conserved sites could produce viral escape variants, mAbs targeting these sites may
95 nevertheless serve as prophylactics for high-risk populations.
96

97 **RESULTS**

98 **Isolation of broad H1 and H3 monoclonal antibodies**

99 To identify broad subtype neutralizing mAbs, we used a panel of reporter IAVs spanning
100 1933 to 2021 that includes distinct antigenic clusters[2], representing IAVs that have previously
101 escaped humoral immunity. We sorted single H1-reactive B cells from human PBMCs using
102 recombinant A/California/07/2009 HA (**Supplementary Fig. 1A**). We then sequenced the variable
103 genes, recombinantly produced mAbs[29], and screened for neutralization activity. H1-targeting
104 mAbs were screened against representative H1N1 strains A/WSN/1933, A/Solomon
105 Islands/3/2006, and A/Michigan/45/2015. We identified two clonally related mAbs, ADI-77470

106 and ADI-77474, that completely neutralized (>99%) all three H1N1 viruses at 1 μg/ml used for
107 screening (**Supplementary Fig. 1B**).
108 To isolate broad H3 mAbs, we sorted B cells using recombinant HA probes from H3N2s
109 A/Hong Kong/1/1968 (HK68) and A/Darwin/6/2021 (DAR21) coupled to different streptavidin
110 fluorophore conjugates to identify cross-reactive B cells (**Supplementary Fig. 1C**). The HK68
111 probe included the HA head appended to a foldon trimerization tag, allowing us to isolate head-
112 directed mAbs in addition to those that target full-length DAR21 HA. The frequency of cross-
113 reactive HK68/DAR21 head-reactive memory B cells was rare, ranging from 0.0049 to 0.016%
114 across five donors (**Supplementary Fig. 1C**). We further characterized two H3 mAbs, ADI-85647
115 and ADI-85666 after screening for broad neutralization activity (**Supplementary Fig. 1D**).
116 We characterized the subtypic neutralization potency and breadth of these broad H1 and
117 H3 mAbs against 11 H1N1 or 10 H3N2 IAVs. The broad H1 mAbs potently neutralized all H1N1
118 viruses, but not a representative H3N2; the broad H3 mAbs neutralized all H3N2 viruses, but not
119 a representative H1N1 (**Fig. 1**), demonstrating breadth within but not across subtypes. To further
120 test the breadth of these mAbs, we screened for binding by ELISA to the HA from a swine H1N1
121 with pandemic potential (A/Swine/HN/SN13/2018[30]) or an H3 HA from an avian-origin canine
122 IAV found to evolve mammalian influenza-like traits (A/Canine/Hainan/79/2019[31]). Although
123 these IAVs have never circulated in humans, these mAbs bound these strains, highlighting their
124 considerable breadth (**Fig. 1C**). We performed competition assays to crudely map the region on
125 HA targeted by these mAbs. The broad H1 mAbs competed with 047-09M-2F03[17], a mAb that
126 engages the lateral patch of H1 HAs. ADI-85647, a broad H3 mAb, competed with F005-126[32],
127 H3v-47[15], and c585[21], which target the H3 head, whereas the other H3 mAb, ADI-85666, competed
128 with MEDI8852[9], showing that it engages the stem region (**Fig. 1C**). Consistent with binding the
129 stem, ADI-85666 additionally neutralized a group 2 H7N9 (**Fig. 1B**).
130
131 **Viral escape from broad H1 antibodies targeting the head**
132 We next more finely mapped the recognition of the broad H1 mAbs by viral escape. We
133 previously generated deep mutational scanning viral libraries of three H1N1s containing all single
134 amino acid mutations and deletions in the HA head (residues 52–263, H3 numbering):
135 A/USSR/90/1977 (USSR77), A/Siena/10/1989 (SN89), and A/Solomon Islands/3/2006 (SI06)[33].
136 Here, we additionally generated a viral library on the A/Sydney/5/2021 (SYD21) background to

137 determine whether escape is different in a post-2009 pandemic H1N1 virus (**Supplementary Fig.**
138 **2A**). We determined neutralization potencies of ADI-77470, ADI-77474, and a V-gene germline-
139 reverted ADI-77474 against these libraries (**Supplementary Fig. 2B**). The germline-reverted
140 ADI-77474 showed undetectable neutralization activity, demonstrating the importance of the
141 somatic mutations in these mAbs (**Supplementary Fig. 2B**). We passaged the four viral libraries
142 in the presence of either ADI-77470 or ADI-77474 at 10x the IC_{99} concentration to identify escape
143 variants (**Fig. 2 and Supplementary Fig. 2B**). Mutation of P122 to acidic residues (e.g., Asp, Glu)
144 or deletion were the most selected in all virus backgrounds (**Fig. 2C and Supplementary Fig.**
145 **2F**). However, ADI-77474 was more sensitive to mutational escape in SYD21 compared to its
146 clonal relative ADI-77470 (**Fig. 2 and Supplementary Fig. 2**). Although escape primarily
147 occurred at position 122, mutation to Asn at 122, 123, and 124 in SYD21 were selected by both
148 mAbs; each of these Asn mutations introduces a predicted N-linked glycosylation sequon (**Fig. 2C**
149 **and Supplementary Fig. 2F**). Although 123N and 124N mutations in the historical strains
150 USSR77, SN89, and SI06 also create potential N-linked glycosylation sites, these mutations were
151 not enriched in these strains, demonstrating different barriers to escape for pre- and post-pandemic
152 H1s (**Fig. 2C and Supplementary Fig. 2F**). We mapped the escape mutations onto the structure
153 of an HA bound by a mAb engaging the same epitope and that uses the same V-genes[17] (**Fig. 2B**).
154 Residues 119, 122-125, and 172 cluster around the YxR motif often found in this class of mAbs[17];
155 the mAbs we describe have a similarly charged YxK motif in the CDRH3 (**Supplementary Fig.**
156 **3C**). These escape mutations do not overlap with those of Ab6649[33], which targets an overlapping
157 region within the lateral patch.
158
159 **Affinity maturation of broad H1 mAbs increases neutralization potency**
160 To increase the affinity of the broad H1 mAbs, we generated yeast libraries encoding
161 mutations in the variable heavy and light chain genes and selected variants with increased binding
162 affinity using recombinant monomeric SYD21 head[34] (**Supplementary Fig. 3A**). We down-
163 selected affinity-matured mAbs based on a single replicate neutralization screen against SYD21
164 virus (**Supplementary Fig. 3B**) and further tested the most potent of these mAbs against the
165 historical H1N1 A/Beijing/262/1995 (BE95) (**Fig. 3A**). The *in vitro* affinity-matured mAb, ADI-
166 86325, has 2 heavy and 4 light chain mutations relative to ADI-77470 (**Supplementary Fig. 3C**),
167 which increased the potency against SYD21 by ~4-fold while maintaining BE95 neutralization

168 (**Fig. 3A**). We next assessed whether *in vitro* affinity maturation of ADI-77470 to ADI-86325
169 affected viral escape by using deep mutational scanning of the SYD21 virus. We found that
170 mutations that had limited escape effect from ADI-77470 had a reduced effect against ADI-86325,
171 but highly selected escape mutations were nevertheless similar suggesting these residues are
172 critical for HA recognition by these mAbs (**Fig. 2C and 3B**).
173 To determine the occurrence of escape mutations in IAV isolates, we used a previous
174 conservation analysis performed on 1222 unique H1 sequences representative of sequence clusters
175 from 1918–2019[35] to determine whether observed escape mutations have occurred naturally (**Fig.**
176 **3B-D**). Despite some positions with low ConSurf[36] scores, specific amino acid escape mutations
177 have rarely been observed in H1 sequences (**Fig. 3B-D**), suggesting that ADI-86325 is likely to
178 neutralize most H1N1 viruses and providing an explanation for the high degree of neutralization
179 breadth. The identification of escape mutations *in vitro* that have yet to appear naturally possibly
180 suggests that such antibodies have historically been rare within the human population.
181
182 **A broad H3 mAb targets the side of the H3 head**
183 As analogous deep mutational scanning libraries for historical and contemporary H3N2
184 viruses were unavailable, we used cryo-EM to structurally determine the epitopes targeted by the
185 broad H3 mAbs. ADI-85647 in complex with A/Darwin/6/2021 (DAR21) HA shows that it binds
186 to the side of the HA head, consistent with competition with H3v-47, c585, and F005-126 (**Fig. 1**
187 **and 4A**). During antigenic drift of H3N2s, potential N-linked glycosylation sites on HA were
188 acquired and maintained at this site at positions 122, 126, and 133[37]. Although the cryo-EM map
189 showed clear features of a glycan at N133, we did not observe a glycan at N122, consistent with a
190 previous report showing no and full glycan occupancy at N122 and N133, respectively[38]. The
191 N133 glycan sits within a cleft between the variable heavy and light chains of ADI-85647, and the
192 CDRH2 inserts between the N133 and N126 glycans (**Fig. 4B**). The Y32 hydroxyl and V2
193 backbone in the heavy chain form hydrogen bonds with the GlcNAc and one of the branching
194 mannose moieties of the glycan, respectively, and thus stabilize the glycan within this cleft. There
195 are eleven hydrogen bonds, two of which are with the N133 glycan; no salt bridges are present.
196 The heavy chain contributes only two hydrogen bonds in addition to interacting with HA through
197 several aromatic residues (**Fig. 4C**); W102 in the CDRH3 sits within a pocket underneath the 130-

198 loop. While the ADI-85647 epitope significantly overlaps with that of H3v-47 (**Fig. 4D**), ADI-
199 85647 can also bind and neutralize H3N2 strains prior to 1989 in contrast to H3v-47[15].
200
201 **Group 2 neutralization through a unique structural solution**
202 The anti-stem mAb ADI-85666 uses the germline genes V_H4-61 and V_K1-17, which have
203 not been previously reported for group 2 anti-stem mAbs; we therefore determined a cryo-EM
204 structure bound to DAR21 HA_0 to understand how recognition differs from previously reported
205 mAbs (**Fig. 5A**). The epitope overlaps with recognition of other group 2 neutralizing mAbs[10,39],
206 such as CR8020, but in contrast to other group 2 neutralizing mAbs, the CDRH3 of ADI-85666
207 extends into a groove spanning the β-sheet at the base of the stem located near the viral membrane
208 (**Fig. 5B**). The tyrosine at the tip of the CDRH3 makes a stabilizing aromatic-sulfur contact with
209 M133 (HA_2 numbering) (**Fig. 5B**). One side of the CDRH3 interacts with the hydrophobic groove
210 with I107 and F109 in the CDRH3 while the other side forms a Glu-Arg-Tyr triad with R25 of
211 HA. A second Glu-Arg-Tyr triad is formed with E15 of the fusion peptide and residues Y34 and
212 R99 in the CDRH2 and CDRH3, respectively (**Fig. 5B**). Comparison of the interfacing residues of
213 ADI-85666 with CR8020 shows overlap of the outermost β-strand but diverge towards the central
214 strands or G-helix for ADI-85666 or CR8020, respectively (**Fig. 5C**).
215
216 **Conservation and mutational tolerance of broad H3 mAb epitopes**
217 We next mapped conservation and mutational tolerance of the ADI-85647 and ADI-85666
218 epitopes onto the structure of the DAR21 HA (**Fig. 6**). The conservation scores were obtained from
219 a previous ConSurf[36] analysis of 3,408 unique H3 HA sequences representing historical sequence
220 clusters[35]. To assess the potential for viral escape, we also mapped mutational tolerance derived
221 from A/Perth/16/2009 onto the HA structure, which measures whether mutations at each site
222 impact viral fitness[28]. The ADI-85647 footprint contains some highly variable residues (**Fig. 6**),
223 explaining the variable neutralization potencies (**Fig. 1**); the CDRs of ADI-85647, however,
224 mainly interact with historically conserved residues (**Fig. 6**). Tryptophan 102 in the CDRH3
225 interacts with a pocket underneath the receptor binding site that is both historically conserved and
226 mutationally intolerant (**Fig. 6**). The groove contacted by ADI-85666 is moderately conserved, but
227 contains few highly variable residues, explaining the broad and consistent neutralization potency

228 (**Fig. 1**). However, several positions within the ADI-85666 footprint are highly tolerant to
229 mutations, suggesting mutation at these sites may result in viral escape (**Fig. 6**).
230
231 **DISCUSSION**
232 Here, we isolated broad H1 and H3 neutralizing mAbs from human donors and
233 characterized the targeted epitopes by viral escape and cryo-EM, respectively. Broad H1 mAbs
234 potently neutralize all tested H1N1 strains from 1933 to 2021 and bind to a pre-pandemic swine
235 HA. Despite conservation of the lateral patch recognized by broad H1 mAbs, viral escape occurred
236 readily, primarily at position 122. We engineered the broad H1 mAbs for increased affinity to a
237 contemporary HA, increasing neutralization potency ~4-fold. This affinity-matured mAb, ADI-
238 86325, selected for viral escape mutations P122D/E/-, 125D/E, and Asn mutations at 122-124,
239 which introduce potential N-linked glycosylation sites; however, these mutations are rarely
240 observed in human IAV isolates. Structural characterization of the broad H3 anti-head mAb, ADI-
241 85647, suggests that engagement of a conserved pocket underneath the 130-loop of the receptor
242 binding site is a target for broad H3 mAbs. The structure of the group 2 anti-stem mAb, ADI-
243 85666, shows the CDRH3 inserts into a groove not contacted by previously characterized group 2
244 anti-stem mAbs. Comparing these epitopes with previous deep mutational scanning data suggests
245 potential viral escape should this type of antibody response become dominant[28].
246 The 2009 H1N1 pandemic initially recalled cross-reactive B cell responses that targeted
247 the RBS and lateral patch[17,22,40]. However, upon subsequent exposures, these responses were
248 absent[17], which likely contributes to the continued conservation of the lateral patch epitope. Next-
249 generation vaccines using mosaic nanoparticles containing antigenically distinct H1 HA heads
250 elicit antibodies targeting the lateral patch in animal models[25,26]. In humans, initial recall of lateral
251 patch-directed mAbs after the pandemic selected for viral escape through an N-linked
252 glycosylation[22]. However, a subset of lateral patch-directed mAbs, primarily encoded by V_H3-
253 23/V_K1-33, can overcome this escape. It is possible that these mosaic nanoparticle vaccine
254 candidates in humans may preferentially elicit V_H3-23/V_K1-33 responses targeting the lateral
255 patch. The two clonally related mAbs encoded by V_H3-23/V_K1-33 genes we identified here elicited
256 escape at positions engaged by the common CDRH3 motif in this class of mAb (119, 122, 125,
257 and 172), mostly independent of the background strain. Despite further affinity maturation, these
258 mAbs were still readily escaped by mutations at the same positions in contrast to affinity

259 maturation of RBS-directed mAbs that we have previously shown can prevent escape at certain
260 positions[33]. These data suggest that next-generation vaccines eliciting antibodies targeting this site
261 may not provide long-term, broad protection. However, if population-wide immune pressure on
262 this site does not increase, lateral patch mAbs may nevertheless serve as potent prophylactics or
263 therapeutics for high-risk populations. Further studies are needed to understand whether there are
264 mAbs that target this site and are insensitive to the escape mutations described here while
265 maintaining their broad reactivity.

266 Comparison of the structures of ADI-85647 and H3v-47 show that both insert hydrophobic
267 residues into a conserved pocket underneath the 130-loop. ADI-85647, but not H3v-47, recognizes
268 strains prior to 1989[15], highlighting that these mAbs are sensitive to different mutations within this
269 epitope despite largely overlapping footprints. As shown previously, the H3 head domain appears
270 to be more mutationally intolerant than the stem; this contrasts with H1 HAs[28]. This conservation
271 and mutational intolerance within the pocket engaged by these mAbs may be a result of the
272 proximity to the conserved W153 in the receptor binding pocket; therefore, mAbs engaging this
273 pocket with different V-genes, angles of approach, and mutation sensitives may be an additional
274 way to target H3N2s with escape resistance; reminiscent of a polyclonal antibody response to the
275 RBS pocket[23]. Although ADI-85647 targets a site on H3 like that targeted by H1 lateral patch
276 mAbs, the neutralization potency is markedly lower. While *in vitro* affinity maturation of ADI-
277 85647 may increase potency, it is possible that H1N1 and H3N2 viruses are differentially
278 neutralized by broad mAbs targeting these sites or that the potency of mAbs targeting these sites
279 are dependent on the angle of approach.

280 The group 2 mAb, ADI-85666, targets an epitope that overlaps with that of other group 2
281 neutralizing mAbs, CR8020[10] and CR8043[39], but has an extended CDRH3 that reaches into a
282 groove not contacted by other mAbs; this is the third structurally characterized group 2 mAb that
283 engages this site, each with distinct epitopes. The varied gene usage and diversity of recognition
284 suggests that a polyclonal antibody response to this site may be resistant to escape. We note,
285 however, that a recent clinical trial of a prophylactic pan-influenza stem-targeting mAb, VIR2482,
286 failed to significantly reduce IAV illness (NCT05567783). Therefore, although we do not expect
287 group 2 stem-directed mAbs, or vaccines that elicit them, to prevent infection, they may afford an
288 important bridge during seasons of large antigenic change or in the case of spillover of a subtype
289 for which humans have limited immunity. Together, these broad subtypic neutralizing mAbs could

290 be used as prophylactics or therapeutics. Additionally, these mAbs, the viral escape mutations, and
291 structurally characterized epitopes can be used as tools for designing next-generation vaccines for
292 broad protection.
293
294 **MATERIALS AND METHODS**
295
296 **Human B cell sorting**
297 H1 and H3 antigen-specific B cells were detected using recombinant biotinylated H1 and
298 H3 antigens tetramerized with fluorophore-conjugated streptavidin (SA) as previously described[41].
299 Briefly, His-tagged H1N1 A/California/04/2009 full length trimer Y97F (Sino Biological Cat #
300 11055-V08B1) was mixed in 4:1 molar ratios with SA-Allophycocyanin (APC; Invitrogen) and
301 SA phycoerythrin (PE; Invitrogen) while A/Darwin/6/2021 full-length soluble trimer and A/Hong
302 Kong/1/1968 head trimer (see below) were mixed in 4:1 molar ratios with SA phycoerythrin (PE;
303 Invitrogen) and SA- Allophycocyanin (APC; Invitrogen), respectively, and were incubated for 20
304 min on ice. B cells were isolated using a Pan B cell isolation kit (Miltenyi Cat#130-101-638) from
305 approximately 10 million PBMCs and stained with tetramerized antigens (25 nM each); anti-
306 human antibodies anti-CD19 (PE-Cy7; Clone HIB19; Biolegend Cat # 302216), anti-CD3 (PerCP-
307 Cy5.5; CloneOKT3; Biolegend Cat # 317335), anti-CD8 (PerCP-Cy5.5; Clone SK1; Biolegend
308 Cat # 344710), anti-CD14 (PerCP-Cy5.5; Clone 61D3; Invitrogen Cat # 45-0149-42), and anti-
309 CD16 (PerCP-Cy5.5; Clone B73.1; Biolegend Cat # 360712); and 50 µl Brilliant Stain Buffer (BD
310 BioSciences) diluted in FACS buffer (2% BSA/1mM EDTA in 1X PBS). All antibodies were used
311 at 1:100 dilutions and cells were incubated for 15 min on ice. After one wash with FACS buffer,
312 cells were stained in a mixture of propidium iodide and anti-human antibodies anti-IgG (BV605;
313 Clone G18–145; BD Biosciences Cat # 563246), anti-IgA (FITC; Abcam Cat # Ab98553), anti-
314 CD27 (BV510; Clone MT271; BD Biosciences Cat # 740167), and anti-CD71 (APC-Cy7; Clone
315 CY1G4; Biolegend Cat # 334110). Following 15 min of incubation on ice, cells were washed two
316 times with FACS buffer and analyzed using a BD FACS Fusion (BD BioSciences). For sorting of
317 H1/H3-specific, class-switched B cells, B cells that react with H1N1 A/California/04/2009 full
318 length trimer Y97F tetramers or A/Hong Kong/1/1968 head trimer and A/Hong Kong/1/1968 head
319 trimer tetramers among CD19+CD3−CD8− CD14−CD16−PI− and IgG+ or IgA+ cells were
320 single-cell index sorted into 96-well polystyrene microplates (Corning) containing 20 µl lysis

321 buffer per well [5 µl of 5X first strand SSIV cDNA buffer (Invitrogen), 1.25 µl dithiothreitol (0.1
322 M, Invitrogen), 0.625 µl of NP-40 (Thermo Scientific), 0.25 µl RNaseOUT (Invitrogen), and 12.8
323 µl dH2O]. Plates were briefly centrifuged and then frozen at −80 °C before PCR amplification.
324
325 **Cell lines and media**
326 Cell lines HEK293T, HEK293T-PB1, MDCK-SIAT1-PB1, and MDCK-SIAT1-H7 (gifts
327 from Jesse Bloom and Masaru Kanekiyo) were maintained in DMEM (Gibco) with 10% heat-
328 inactivated FBS (Peak), and penicillin/streptomycin (Gibco). For the growth of MDCK-SIAT1-
329 PB1 and MDCK-SIAT1-H7 cells, 1 mg/ml geneticin (Gibco) and 0.25 µg/ml puromycin (Gibco)
330 were additionally added. For neutralization assays, "flu media" was used, which contains Opti-
331 MEM (Gibco), 0.3% BSA (Sigma), penicillin/streptomycin, 0.1 mg/ml $CaCl_2$, and 0.01% heat-
332 inactivated FBS (Peak).
333
334 **Generation of influenza reporter viruses**
335 Influenza reporter viruses were generated as described previously[42] based on the methods
336 from Creanga et al.[35]. Briefly, reverse genetics bidirectional pHW plasmids (some of which were
337 gifts from Jesse Bloom and Masaru Kanekiyo) encoding the HA and NA of each strain, the internal
338 segments (except PB1) from A/WSN/1933 (for H1N1 viruses) or A/Netherlands/009/2010 (for
339 H3N2 viruses), tdKatushka2 with PB1 packing sequences, and a plasmid that drives expression of
340 human TMPRSS2 were transfected into a co-culture of HEK293T-PB1 (a gift from Jesse Bloom)
341 and MDCK-SIAT1-PB1 cells (a gift from Masaru Kanekiyo) in 6-well plates using TransIT-LT1
342 (MirusBio) at a 2:1 ratio. For H1N1s, the non-coding regions from A/WSN/1933 were used and
343 for H3N2s, the non-coding regions from A/Netherlands/009/2010 were used. The virus-containing
344 supernatant was harvested after three days, clarified by centrifugation, and added to a confluent
345 monolayer of MDCK-SIAT1-PB1 cells seeded the day prior. Once cytopathic effect was evident
346 (two to three days), the supernatant was clarified and stored at -80 °C. To safely generate an H7N9
347 A/Shanghai/02/2013 virus in a BSL2 setting, we used pHW plasmids encoding tdKatushka with
348 HA packing sequences, the A/Shanghai/02/103 NA, the internal genes from mouse-adapted PR8,
349 and a plasmid that expresses full-length H7 HA from A/Shanghai/02/2013, but lacks non-coding
350 regions. This virus was propagated using the MDCK-SIAT-H7 cell line (a gift from Masaru
351 Kanekiyo) that constitutively expresses cell-surface H7 A/Shanghai/02/2013 HA.

352

353 **Microneutralization assays**

354 Neutralization assays were performed as previously reported[43] based on a previously
355 developed assay[35]. Briefly, MDCK-SIAT1-PB1 (or MDCK-SIAT1-H7 for H7N9 neutralization
356 assays) cells were seeded in 96-well plates (Cellvis, #P96-1.5P) at 20,000-30,000 cells per well in
357 100 µl of flu media. The next day, viruses were diluted in flu media containing 2 µg/ml TPCK-
358 trypsin and antibodies were diluted separately in flu media at 2-20 µg/ml for screening or titrated
359 to determine IC_{50} values. The virus and antibody dilutions were mixed at a 1:1 ratio (60 µl : 60 µl)
360 and incubated (37 °C / 5% CO_2) for 1 hour. Then, the flu media was removed from the MDCK-
361 SIAT1-PB1 (or -H7) cells and 100 µl of the antibody/virus mixture was overlayed on top of the
362 cells. Approximately eighteen hours later, the plate was imaged for tdKatushka2 fluorescence
363 using a Zeiss CellDiscoverer7 and fluorescent cells were counted using Zeiss Zen software. The
364 average counts of the virus control wells (no antibody added) determined 0% neutralization and
365 cell only control wells (no virus added) determined 100% neutralization. The neutralization values
366 were plotted in GraphPad Prism and IC_{50} values were determined by a sigmoidal curve fit.

367

368 Antibodies used for deep viral escape selections were also titrated on the libraries to
369 determine concentrations to use in selections as described previously[33]. Briefly, 20,000-30,000
370 humanized MDCK (hCK) cells[44] were seeded in 96-well plates overnight in flu media. Viruses
371 were then diluted in half-log dilutions for titering or to 200 TCID50 / 50 µl for neutralization
372 assays. For neutralization assays, four-fold antibody dilutions were then added and complexed
373 with virus (1 hour / 37 °C / 5% CO_2). After 1 hour, the antibody/virus mixture was removed and
374 the cells were washed with PBS before adding fresh flu media with 1 µg/ml TPCK-trypsin. After
375 18 hours, the cells were fixed with cold 80% acetone in PBS for 10 minutes and air-dried. The
376 wells were washed with PBS + 0.3% Tween20 and blocked with PBS + 0.1% Tween20 + 1% BSA
377 (1 hour, room temperature). The wells were again washed and a mixture of anti-nucleoprotein
378 mAbs (Sigma) were added (1 hour, room temperature). The wells were washed again before adding
379 anti-mouse antibody HRP conjugate (seracare) (1 hour, room temperature). Prior to adding Ultra
380 TMB (ThermoFisher), the wells were washed 5 times. The development of TMB was stopped by
381 addition of 2M sulfuric acid and the resulting absorbance was read at 450 nm. $TCID_{50}$ values were
382 determined by the Reed and Muench method[45] using 4-8 replicates. Neutralization IC_{50} values

383 were calculated by sigmoidal curve fit in GraphPad Prism and IC_{99} values were then calculated by
384 $IC_{99} = (99/(100-99))^{(1/\text{hill slope})} \times IC_{50}$.
385
386 **ELISA**
387 Recombinant full-length soluble ectodomain HA (see below) was coated on high binding
388 96-well plates (Corning) at a concentration of 2 µg/ml overnight at 4 °C. The antigen was then
389 removed and wells were blocked with PBS + 1% BSA + 0.1% Tween20 (1 hour, room
390 temperature). The blocking buffer was removed and 40 µl of antibody was added at 10 or 1 µg/ml
391 to screen for binding (1 hour, room temperature). The antibodies were removed, and the wells were
392 washed three times with PBS + 0.1% Tween20. Anti-human IgG HRP conjugate (Abcam) was
393 then added (1 hour, room temperature). The wells were then washed three times with PBS + 0.1%
394 Tween20 and One Step ABTS was added before reading absorbance at 405 nm. The average of
395 multiple wells with PBS added instead of primary antibody was used to as a background
396 measurement.
397
398 **BLI competition assay**
399 Epitope competition binning of mAbs was assessed using the ForteBio Octet HTX
400 (Sartorious). All protein reagents were diluted in PBSF (PBS+0.1% BSA). Anti-human capture
401 (ACH) sensor tips were loaded for 180 seconds with test IgGs at 300 nM. Next, tips were
402 transferred to wells for 180 seconds containing 300 nM soluble HA trimer. After antigen binding,
403 tips were transferred to wells containing test IgGs at 100 nM for 180 seconds to ensure complete
404 blocking of the antigen epitopes of these mAbs. In the last step, sensor tips were transferred to
405 wells containing control IgGs at 100 nM for 180 seconds. An observable binding response in the
406 last step indicates non-competition whereas no observable binding response indicates competition.
407 Data were analyzed using ForteBio Octet BLI analysis software version 12.2.13.5.
408
409 **Influenza HA plasmid library generation**
410 Influenza HA library cloning and viral generation was performed as previously described[33].
411 A deep mutational scanning library encoding all possible single amino acid mutations (Twist
412 Bioscience), including deletions, in the HA head (H3 numbering 52-263) of A/Sydney/5/2021 was
413 assembled using golden gate cloning (BsmBI-v2 Golden Gate Mix, NEB) with a barcoded segment

414 into pDM_RevGen068, a modified pHW2000 containing a GFP insert to detect background
415 colonies during library cloning. After assembly, the reaction was dialyzed prior to electroporation
416 into NEB 10-beta cells. After 1 hour of recovery, the cells were plated on large agar plates and
417 ~200,000 colonies were scraped, cultured in LB supplemented with carbenicillin for 2 hours before
418 isolating the plasmid library by maxiprep (Macherey-Nagel).
419
420 **PacBio sequencing**
421 To link the barcodes with individual amino acid variants, PacBio sequencing of SalI-
422 digested plasmid was performed by the Bauer core using a SMRTbell v3.0 kit and Pacbio Sequel
423 IIe sequencer. Computational methods to link barcodes with amino acid variants was performed
424 exactly as described in Maurer et al.[33], which is based on previous SARS-CoV-2 RBD deep
425 mutational scanning efforts[46,47].
426
427 **Deep viral escape assay**
428 In T150 flasks with hCK cells (50,000 cells per cm^2 seeded the day prior in flu media),
429 virus libraries were combined with antibody at 10x the calculated IC_{99} value in 28 mls of flu media
430 with 1 µg/ml TPCK-trypsin and incubated (1 hour / 37 °C / 5% CO_2). The media was then removed
431 from hCK cells and the virus/antibody mixture was added for 1 hour (37 °C / 5% CO_2) before
432 removing the inoculum, washing with PBS, and adding fresh flu media with 1 µg/ml TPCK-
433 trypsin. The next day (~20-24 hours), dead cells and cell debris were removed from the supernatant
434 by centrifugation and 20 mls of clarified supernatant was concentrated with a 100K MWCO
435 concentrator (ThermoFisher). The viral RNA was then extracted with a QIAamp viral RNA mini
436 prep (Qiagen).
437
438 **Viral barcode amplification**
439 Barcode amplification was performed as previously described[33]. One µl ezDNase buffer
440 and 1 µl ezDNase was added to 8 µl of viral RNA and incubated at 37 °C for 2 minutes. Then, 1
441 µl dNTPs (10 mM), 1 µl water, and a primer specific for the 3' NCR (prDM370) was added. The
442 mixture was incubated for 5 minutes at 65 °C followed by ice for 1 minute. To this mixture, 1 µl
443 SuperScript IV, 4 µl SuperScript IV buffer, 1 µl RNaseOUT, and 1 µl DTT were added and the
444 reaction was incubated at 50 °C for 30 minutes and then 80 °C for 10 minutes. The cDNA was

445 purified by a 1.6X AMPure XP bead cleanup (Beckman). The cDNA was amplified in two PCR
446 steps. The first PCR step combined 20 µl cDNA, 10 µl Q5 buffer, 1 µl dNTPs, 13.5 µl water, 2.5
447 µl each primer, and 0.5 µl Q5 polymerase. The cycling conditions for the first PCR step were 98
448 °C for 30 seconds; four cycles of 98 °C for 10s, 67 °C for 10s, 72 °C for 10s; 72 °C for 2 minutes.
449 The first PCR was purified by a 1.6X AMPure XP bead cleanup. The second PCR step combined
450 20 µl PCR1 product, 10 µl Q5 buffer, 1 µl dNTPs, 13.5 µl water, 5 µl NEBNext unique dual index
451 primers, and 0.5 µl Q5 polymerase. The cycling conditions for the second PCR step were 98 °C
452 for 30s; 14 cycles of 98 °C for 10s, 72 °C for 15s; 72 °C for 2 minutes. After purification with
453 AMPure XP beads, the product was analyzed by a D1000 tapestation, and combined at equimolar
454 concentrations before quantifying with Qubit and submitting for sequencing on a NovaSeq SP
455 (Bauer Core).
456
457 **Protein production**
458 Antibodies used in selections and recombinant HAs (head or full-length soluble
459 ectodomain) were cloned into a pVRC8400 (Vaccine Research Center, NIAID, Bethesda, MD)
460 backbone. All proteins contained a His-tag and were purified by cobalt chromatography followed
461 by FPLC purification on S200 column using an AKTA Pure. All proteins, except for the
462 A/Darwin/6/2021 HA trimer, were produced in HEK293F by transfecting with PEI (3:1 ratio) or
463 Expi-293F (ThermoFisher) cells following the manufacturer's recommended transfection
464 protocol. Full-length soluble ectodomain trimers, except for the A/Darwin/6/2021 HA trimer used
465 in cryo-EM, contained a foldon trimerization tag. The A/Darwin/6/2021 HA trimer used for cryo-
466 EM was produced in Expi293F GnTI- cells and contained three stabilizing mutations in the stem:
467 H26W, K51I, and E103I[48]. Proteins used for B cell sorting and yeast-based affinity maturation
468 were biotinylated by amine coupling and quantified using the QuantTag biotin kit (Vector
469 Laboratories, #BDK-200). Antibodies used for screening, as well as ADI-86325 used in deep
470 mutational scanning selections, were produced in yeast. Expression and purification of IgGs in
471 yeast were produced as full-length IgG1 proteins in S. cerevisiae cultures, as previously
472 described[49]. Briefly, yeast cultures were incubated in 24-well plates placed in Infors Multitron
473 shaking incubators at 30 °C, 650 rpm, and 80% relative humidity. After 6 days, the supernatants
474 containing the IgGs were harvested by centrifugation and purified by protein A-affinity

475 chromatography. The bound IgGs were eluted with 200 mM acetic acid with 50 mM NaCl (pH
476 3.5) into 1/8 [v/v] 2 M HEPES (pH 8.0) and buffer-exchanged into PBS (pH 7.0).
477
478 **Yeast-based affinity maturation**
479 Affinity maturation libraries were generated as described previously[50]. Overlap extension
480 PCR was used to incorporate NNK codons into the complementary determining regions (CDRs)
481 of the variable heavy- and light-chains. Variable heavy and light chain libraries were generated
482 separately and recombined in heavy chain or light chain libraries in yeast by homologous
483 recombination with a linearized plasmid to create yeast libraries of ~1 x 10^7 by electroporation. To
484 prepare S. cerevisiae yeast for electroporation, cells were first grown overnight in YPD media and
485 refreshed the morning of electroporation to 0.5 OD600 in YPD for 4 hours. Yeast cells were then
486 collected and washed twice with sterile water before incubating in 0.1 M lithium acetate / 10 mM
487 DTT for 10 minutes. The yeast cells were then washed twice with ice-cold water and resuspended
488 in ice-cold 10 mM lithium acetate. The insert and plasmid DNA were added to the yeast cells and
489 electroporated at 0.5 kV / 2000 µF. YPD media was used to recover the cells before incubating at
490 30 °C. The yeast cells were then resuspended in SDCAA media (6.7 g/L Yeast Nitrogen Base, 4.0
491 g/L drop out amino acid mix, 7.3 g/L NaH2PO4, 5.4 g/L Na2HPO4, 4% w/v dextrose) and grown
492 at 30 °C. The heavy- and light-chain libraries were selected over two rounds for binding to
493 recombinant A/Sydney/5/2021 HA head monomer. The number of yeast cells stained in each
494 selection was at least 10-fold the library diversity. Each library was incubated with either 10 or 1
495 nM of biotinylated SYD21 HA head monomer under equilibrium conditions. The yeast cells were
496 washed twice in PBSF (1x PBS, 0.1% [w/v] BSA) before staining with anti-human LC-FITC
497 (Southern Biotech), Streptavidin 633 (Invitrogen), and propidium iodide (Invitrogen) for 15
498 minutes on ice. The yeast cells were washed twice and resuspended in PBSF before sorting on a
499 BD FACS Aria II. Yeast cells showing improved antigen binding over parental clones were sorted
500 in each round. After two rounds of sorting, the outputs from the heavy- and light-chain libraries
501 were combined to generate a library of clone with diversity across all CDRs. This library was also
502 sorted for two rounds before plating the yeast on SDCAA agar plates for single clone isolation and
503 sequencing.
504
505 **HA conservation and mutational tolerance analyses**

506 For the pairwise identity maps shown in Figure 1, HA sequences of reporter viruses used
507 in this study were aligned and pairwise identity was calculated in Geneious. For conservation
508 analyses of H1 and H3 HAs we used a previous analysis[35] of 1222 unique H1 or 3408 unique H3
509 HA sequences from the GISAID database[51], removing duplicates or sequences with poor
510 sequencing data, performing clustering using CD-HIT EST[52], and selecting representative
511 sequences from these clusters. Cluster representatives were then analyzed for conservation using
512 ConSurf[36]. For mutational tolerance analyses, we used the entropy values from Lee et al.[28]. Color
513 spectrums were obtained from colorbrewer2.org. Antibody footprints were determined by
514 interfacing residues from PISA[53].
515
516 **Cryo-EM sample preparation and data collection**
517 The recombinant HA (rHA) full length soluble ectodomain (FLsE) of A/Darwin/6/2021
518 (H3N2) was incubated with ADI-85647 or ADI-85666 Fab at a molar ratio 1:1 and a final protein
519 concentration of 2.5 mg/ml for 40 minutes on ice. Immediately before depositing the sample onto
520 Quantifoil R0.6/1, 3400 mesh gold grids coated with 2nm continuous carbon, octyl-beta-glucoside
521 was added to the pre-formed complex at 0.083% (w/v) final concentration. Plasma cleaning of the
522 grids was performed with a Solarus plasma cleaner machine (Gatan) for 30 seconds (H2, O2).
523 Three microliters of the sample were applied on the continuous carbon face of the grids, blotted
524 for 5.5 seconds on the same face of the grid, at 20˚ C and 80% humidity, then plunge-frozen in
525 100% liquid ethane using a Leica EM GP2 plunge freezer. The grids were first screened on an
526 Artica Talos microscope equipped with a Gatan K3 camera and operated at 200 kV. The highest
527 quality grid was then imaged using a Titan Krios microscope operated at 300 kV and equipped
528 with a Gatan K3 Summit direct electron detector. A total of 7,772 and 4,435 movies for the ADI-
529 85647 or ADI-85666 complex, respectively, were collected in counting mode at 30 e-/px/s for a
530 total dose of 52.44 $e^{-}/Å^{2}/s$. Images were collected at a magnification of 81000, corresponding to a
531 calibrated pixel size of 0.825 Å/pixel. Defocus values ranged between -1 and -2.5 µm.
532
533 **Cryo-EM data processing**
534 The data were processed (**Supplementary Figs. 4 and 5**) using cryoSPARC v4.3.1[54].
535 Briefly, the movies were aligned and corrected for both global and local motion using Patch
536 Motion Correction within cryoSPARC. Then, contrast transfer function estimation was done using

537 Patch CTF and particles were picked using template picker. The picked particles were extracted
538 with a box size 400 pixels and 4x binned for 2D classification. Two rounds of 2D classification
539 were performed and the good particles were selected for the generation of the initial model at 12
540 Å/pixel with 3 classes. Non-uniform refinement was performed in C1 symmetry for each
541 individual class. The particles from the best class were re-extracted with a box size of 400 pixels
542 and binned 2x and then subject to 3D classification into 3 classes with a target resolution of 4Å.
543 The particles from the top class were combined and used for non-uniform refinement and local
544 CTF refinement with the best volume obtained from the 3D classification. The particle stack from
545 the local CTF refinement was then used for new round of non-uniform refinement, and then a new
546 round of 3D classification was performed with 3 classes at a target resolution of 3Å. The 3 classes
547 were subject to a new round of non-uniform refinement. Local CTF refinement was then performed
548 the final particle stack and then subjected to a new round of non-uniform refinement with C3
549 symmetry imposed. A new round of local CTF refinement followed by non-uniform refinement in
550 C3 symmetry was performed and then subject to global CTF refinement follow by new round of
551 non-uniform refinement in C3 symmetry. The particles were re-extracted at full box size of 400
552 pixels without binning and a new round of non-uniform refinement and local CTF refinement was
553 performed. This particle stack was used for a last non-uniform refinement with C3 symmetry and
554 yielded a reconstruction at 3Å nominal resolution. The two half-maps were used for sharpening in
555 DeepEMhancer[55]. The reported resolution is based on the gold-standard Fourier shell correlation
556 of 0.143 criterion.
557
558 **Model building and refinement**
559 The DeepEMhancer sharpened maps were used for model building with ModelAngelo[56]
560 and then manually built using COOT[57]. N-linked glycans were built manually in COOT using the
561 glyco extension and their stereochemistry and fit to the map validated with Privateer[58]. The models
562 were then refined in Phenix[59] using real-space refinement and validated with MolProbity[60].
563
564 **Computational sequencing analyses**
565 Computational sequencing analyses were performed exactly as described in Maurer et al.[33].
566 Briefly, barcodes and amino acid variants were linked from PacBio sequencing using *alignparse*[61].
567 Variants with insertions were removed from analysis. Sequences with ≥3 PacBio CCSs per

568 barcode were retained for analysis. After amplification of the barcodes, paired ends were merged
569 with PEAR[62], merged reads were filtered for the correct lengths, and sequences with ambiguous
570 base calls were removed. Unique barcode-UMI combinations were used for counting. The
571 functional scores were calculated using *dms_variants* (https://jbloomlab.github.io/dms_variants/)
572 comparing the change in variant frequency from the plasmid libraries to after the low MOI (0.01)
573 passage. Relative escape values are derived from differential selection
574 (https://jbloomlab.github.io/dms_tools2/diffsel.html) using a pseudocount of 10. For analysis, we
575 filtered for variants that were positively selected in both independent replicates and set other
576 variants to 0. Relative escape values are normalized to the most selected variant in each selection.
577 These relative escape values are summed by position to obtain a "summed relative escape" value.
578

579 **Data and code availability**

580 Raw sequencing data have been deposited to NCBI in BioProjects PRJNA1130551 and
581 PRJNA1056469. All code used for the analyses here and the resulting output files used to generate
582 the figures can be found at https://github.com/dpmaurer/flu_ab_escape. Atomic models have been
583 deposited to the PDB under accession codes 8BDF and 8BDG and the corresponding maps have
584 been deposited to the EMDB under accession codes EMD-44451 and EMD-44452. Aligned
585 micrographs for these datasets can be found in EMPIAR under accession codes EMPIAR-12059
586 and EMPIAR-12060.
587

588 **ACKNOWLEDGMENTS**

589 At Adimab, we thank the sequencing and yeast antibody production teams, as well as Irina
590 Burina and Elizabeth McGurk for BLI competition assays. We thank Jesse Bloom for providing
591 pHW plasmids. We thank Masaru Kanekiyo for providing the HA and NA plasmids used to
592 generate the reporter viruses and for the cell lines used to propagate the reporter viruses. We thank
593 Adrian Creanga for providing the ConSurf analyses. We acknowledge support from P01 AI089618
594 (A.G.S). This research has been funded in whole or part with federal funds under a contract from
595 the National Institute of Allergy and Infectious Diseases, NIH contract 75N93019C00050 (A.G.S.
596 and G.B.). We also acknowledge support from the Irma T. Hirschl/Monique Weill-Caulier Trust
597 (G.B.). Some of this work was performed at the National Center for CryoEM Access and Training
598 (NCCAT) and the Simons Electron Microscopy Center located at the New York Structural Biology

599 Center, supported by the NIH Common Fund Transformative High Resolution Cryo-Electron
600 Microscopy program (U24 GM129539), and by grants from the Simons Foundation (SF349247)
601 and NY State Assembly.
602
603 **AUTHOR INFORMATION**
604
605 **Author Contributions** D.P.M. and M.V. produced recombinant proteins, performed ELISAs, and
606 performed virus neutralization assays. D.P.M. performed deep mutational scanning assays and
607 analyses. H.L.D., P.K., and J.C.G. sorted human B cells and performed *in vitro* affinity maturation.
608 A.S.F.R. and G.B. determined cryo-EM structures. D.P.M. and A.G.S. wrote the original drafts of
609 the paper. All authors reviewed and commented on the paper.
610
611 **Correspondence and requests for materials should be addressed to:** Aaron G. Schmidt
612 (aschmidt@crystal.harvard.edu)
613
614 **Competing financial interest:** D.P.M., H.L.D., P.K., J.C.G, and L.M.W. are shareholders of
615 Adimab, LLC. P.K. is an employee of Adimab, LLC.
616
617

618 **REFERENCES**

619 1 Wei, C. J. *et al.* Next-generation influenza vaccines: opportunities and challenges. *Nat Rev*
620 *Drug Discov* **19**, 239-252 (2020). https://doi.org/10.1038/s41573-019-0056-x
621 2 Bedford, T. *et al.* Integrating influenza antigenic dynamics with molecular evolution. *Elife* **3**,
622 e01914 (2014). https://doi.org/10.7554/eLife.01914
623 3 Black, S. *et al.* Hemagglutination inhibition antibody titers as a correlate of protection for
624 inactivated influenza vaccines in children. *Pediatr Infect Dis J* **30**, 1081-1085 (2011).
625 https://doi.org/10.1097/INF.0b013e3182367662
626 4 Hobson, D., Curry, R. L., Beare, A. S. & Ward-Gardner, A. The role of serum
627 haemagglutination-inhibiting antibody in protection against challenge infection with
628 influenza A2 and B viruses. *J Hyg (Lond)* **70**, 767-777 (1972).
629 https://doi.org/10.1017/s0022172400022610
630 5 Coudeville, L. *et al.* Relationship between haemagglutination-inhibiting antibody titres and
631 clinical protection against influenza: development and application of a bayesian random-
632 effects model. *BMC Med Res Methodol* **10**, 18 (2010). https://doi.org/10.1186/1471-2288-
633 10-18
634 6 Corti, D. *et al.* A neutralizing antibody selected from plasma cells that binds to group 1 and
635 group 2 influenza A hemagglutinins. *Science* **333**, 850-856 (2011).
636 https://doi.org/10.1126/science.1205669
637 7 Dreyfus, C. *et al.* Highly conserved protective epitopes on influenza B viruses. *Science* **337**,
638 1343-1348 (2012). https://doi.org/10.1126/science.1222908
639 8 Ekiert, D. C. *et al.* Antibody recognition of a highly conserved influenza virus epitope.
640 *Science* **324**, 246-251 (2009). https://doi.org/10.1126/science.1171491
641 9 Kallewaard, N. L. *et al.* Structure and Function Analysis of an Antibody Recognizing All
642 Influenza A Subtypes. *Cell* **166**, 596-608 (2016).
643 https://doi.org/10.1016/j.cell.2016.05.073
644 10 Ekiert, D. C. *et al.* A highly conserved neutralizing epitope on group 2 influenza A viruses.
645 *Science* **333**, 843-850 (2011). https://doi.org/10.1126/science.1204839
646 11 DiLillo, D. J., Palese, P., Wilson, P. C. & Ravetch, J. V. Broadly neutralizing anti-influenza
647 antibodies require Fc receptor engagement for in vivo protection. *J Clin Invest* **126**, 605-610
648 (2016). https://doi.org/10.1172/JCI84428
649 12 Christensen, S. R. *et al.* Assessing the Protective Potential of H1N1 Influenza Virus
650 Hemagglutinin Head and Stalk Antibodies in Humans. *J Virol* **93** (2019).
651 https://doi.org/10.1128/JVI.02134-18
652 13 Koel, B. F. *et al.* Substitutions near the receptor binding site determine major antigenic
653 change during influenza virus evolution. *Science* **342**, 976-979 (2013).
654 https://doi.org/10.1126/science.1244730
655 14 Smith, D. J. *et al.* Mapping the antigenic and genetic evolution of influenza virus. *Science*
656 **305**, 371-376 (2004). https://doi.org/10.1126/science.1097211

657 15 Bangaru, S. *et al.* A multifunctional human monoclonal neutralizing antibody that targets a
658 unique conserved epitope on influenza HA. *Nat Commun* **9**, 2669 (2018).
659 https://doi.org/10.1038/s41467-018-04704-9
660 16 Cheung, C. S. *et al.* Identification and Structure of a Multidonor Class of Head-Directed
661 Influenza-Neutralizing Antibodies Reveal the Mechanism for Its Recurrent Elicitation. *Cell*
662 *Rep* **32**, 108088 (2020). https://doi.org/10.1016/j.celrep.2020.108088
663 17 Guthmiller, J. J. *et al.* First exposure to the pandemic H1N1 virus induced broadly
664 neutralizing antibodies targeting hemagglutinin head epitopes. *Sci Transl Med* **13** (2021).
665 https://doi.org/10.1126/scitranslmed.abg4535
666 18 Krause, J. C. *et al.* A broadly neutralizing human monoclonal antibody that recognizes a
667 conserved, novel epitope on the globular head of the influenza H1N1 virus hemagglutinin. *J*
668 *Virol* **85**, 10905-10908 (2011). https://doi.org/10.1128/JVI.00700-11
669 19 Lee, P. S. *et al.* Receptor mimicry by antibody F045-092 facilitates universal binding to the
670 H3 subtype of influenza virus. *Nat Commun* **5**, 3614 (2014).
671 https://doi.org/10.1038/ncomms4614
672 20 Nogales, A. *et al.* A Highly Potent and Broadly Neutralizing H1 Influenza-Specific Human
673 Monoclonal Antibody. *Sci Rep* **8**, 4374 (2018). https://doi.org/10.1038/s41598-018-
674 22307-8
675 21 Qiu, Y. *et al.* Mapping of a Novel H3-Specific Broadly Neutralizing Monoclonal Antibody
676 Targeting the Hemagglutinin Globular Head Isolated from an Elite Influenza Virus-
677 Immunized Donor Exhibiting Serological Breadth. *J Virol* **94** (2020).
678 https://doi.org/10.1128/JVI.01035-19
679 22 Raymond, D. D. *et al.* Conserved epitope on influenza-virus hemagglutinin head defined by
680 a vaccine-induced antibody. *Proc Natl Acad Sci U S A* **115**, 168-173 (2018).
681 https://doi.org/10.1073/pnas.1715471115
682 23 Schmidt, A. G. *et al.* Viral receptor-binding site antibodies with diverse germline origins.
683 *Cell* **161**, 1026-1034 (2015). https://doi.org/10.1016/j.cell.2015.04.028
684 24 Whittle, J. R. *et al.* Broadly neutralizing human antibody that recognizes the receptor-
685 binding pocket of influenza virus hemagglutinin. *Proc Natl Acad Sci U S A* **108**, 14216-14221
686 (2011). https://doi.org/10.1073/pnas.1111497108
687 25 Dosey, A. *et al.* Combinatorial immune refocusing within the influenza hemagglutinin head
688 elicits cross-neutralizing antibody responses. *bioRxiv* (2023).
689 https://doi.org/10.1101/2023.05.23.541996
690 26 Kanekiyo, M. *et al.* Mosaic nanoparticle display of diverse influenza virus hemagglutinins
691 elicits broad B cell responses. *Nat Immunol* **20**, 362-372 (2019).
692 https://doi.org/10.1038/s41590-018-0305-x
693 27 Portnoff, A. D. *et al.* Influenza Hemagglutinin Nanoparticle Vaccine Elicits Broadly
694 Neutralizing Antibodies against Structurally Distinct Domains of H3N2 HA. *Vaccines (Basel)*
695 **8** (2020). https://doi.org/10.3390/vaccines8010099

696 28 Lee, J. M. *et al.* Deep mutational scanning of hemagglutinin helps predict evolutionary fates
697 of human H3N2 influenza variants. *Proc Natl Acad Sci U S A* **115**, E8276–E8285 (2018).
698 https://doi.org/10.1073/pnas.1806133115
699 29 Bornholdt, Z. A. *et al.* Isolation of potent neutralizing antibodies from a survivor of the 2014
700 Ebola virus outbreak. *Science* **351**, 1078–1083 (2016).
701 https://doi.org/10.1126/science.aad5788
702 30 Sun, H. *et al.* Prevalent Eurasian avian-like H1N1 swine influenza virus with 2009 pandemic
703 viral genes facilitating human infection. *Proc Natl Acad Sci U S A* **117**, 17204–17210 (2020).
704 https://doi.org/10.1073/pnas.1921186117
705 31 Chen, M. *et al.* Increased public health threat of avian-origin H3N2 influenza virus caused by
706 its evolution in dogs. *Elife* **12** (2023). https://doi.org/10.7554/eLife.83470
707 32 Iba, Y. *et al.* Conserved neutralizing epitope at globular head of hemagglutinin in H3N2
708 influenza viruses. *J Virol* **88**, 7130–7144 (2014). https://doi.org/10.1128/JVI.00420-14
709 33 Maurer, D. P., Vu, M. & Schmidt, A. G. Antigenic drift expands viral escape pathways from
710 imprinted host humoral immunity. *bioRxiv* (2024).
711 https://doi.org/10.1101/2024.03.20.585891
712 34 Rappazzo, C. G. *et al.* An Engineered Antibody with Broad Protective Efficacy in Murine
713 Models of SARS and COVID-19. *bioRxiv* (2020).
714 https://doi.org/10.1101/2020.11.17.385500
715 35 Creanga, A. *et al.* A comprehensive influenza reporter virus panel for high-throughput deep
716 profiling of neutralizing antibodies. *Nat Commun* **12**, 1722 (2021).
717 https://doi.org/10.1038/s41467-021-21954-2
718 36 Ashkenazy, H. *et al.* ConSurf 2016: an improved methodology to estimate and visualize
719 evolutionary conservation in macromolecules. *Nucleic Acids Res* **44**, W344–350 (2016).
720 https://doi.org/10.1093/nar/gkw408
721 37 Altman, M. O. *et al.* Human Influenza A Virus Hemagglutinin Glycan Evolution Follows a
722 Temporal Pattern to a Glycan Limit. *mBio* **10** (2019).
723 https://doi.org/10.1128/mBio.00204-19
724 38 Thompson, A. J. *et al.* Human Influenza Virus Hemagglutinins Contain Conserved
725 Oligomannose N-Linked Glycans Allowing Potent Neutralization by Lectins. *Cell Host*
726 *Microbe* **27**, 725–735 e725 (2020). https://doi.org/10.1016/j.chom.2020.03.009
727 39 Friesen, R. H. *et al.* A common solution to group 2 influenza virus neutralization. *Proc Natl*
728 *Acad Sci U S A* **111**, 445–450 (2014). https://doi.org/10.1073/pnas.1319058110
729 40 Wrammert, J. *et al.* Broadly cross-reactive antibodies dominate the human B cell response
730 against 2009 pandemic H1N1 influenza virus infection. *J Exp Med* **208**, 181–193 (2011).
731 https://doi.org/10.1084/jem.20101352
732 41 Kaku, C. I. *et al.* Evolution of antibody immunity following Omicron BA.1 breakthrough
733 infection. *Nat Commun* **14**, 2751 (2023). https://doi.org/10.1038/s41467-023-38345-4

42 Ray, R. *et al.* Eliciting a single amino acid change by vaccination generates antibody protection against group 1 and group 2 influenza A viruses. *Immunity* **57**, 1141–1159 e1111 (2024). https://doi.org/10.1016/j.immuni.2024.03.022

43 Ray, R. *et al.* Eliciting a single amino acid change by vaccination generates antibody protection against group 1 and group 2 influenza A viruses. *Immunity* (2024). https://doi.org/10.1016/j.immuni.2024.03.022

44 Takada, K. *et al.* A humanized MDCK cell line for the efficient isolation and propagation of human influenza viruses. *Nat Microbiol* **4**, 1268–1273 (2019). https://doi.org/10.1038/s41564-019-0433-6

45 REED, L. J. & MUENCH, H. A SIMPLE METHOD OF ESTIMATING FIFTY PER CENT ENDPOINTS12. *American Journal of Epidemiology* **27**, 493–497 (1938). https://doi.org/10.1093/oxfordjournals.aje.a118408

46 Starr, T. N. *et al.* Shifting mutational constraints in the SARS-CoV-2 receptor-binding domain during viral evolution. *Science* **377**, 420–424 (2022). https://doi.org/10.1126/science.abo7896

47 Starr, T. N. *et al.* Deep Mutational Scanning of SARS-CoV-2 Receptor Binding Domain Reveals Constraints on Folding and ACE2 Binding. *Cell* **182**, 1295–1310 e1220 (2020). https://doi.org/10.1016/j.cell.2020.08.012

48 Milder, F. J. *et al.* Universal stabilization of the influenza hemagglutinin by structure-based redesign of the pH switch regions. *Proc Natl Acad Sci U S A* **119** (2022). https://doi.org/10.1073/pnas.2115379119

49 Wec, A. Z. *et al.* Broad neutralization of SARS-related viruses by human monoclonal antibodies. *Science* **369**, 731–736 (2020). https://doi.org/10.1126/science.abc7424

50 Rappazzo, C. G. *et al.* Broad and potent activity against SARS-like viruses by an engineered human monoclonal antibody. *Science* **371**, 823–829 (2021). https://doi.org/10.1126/science.abf4830

51 Shu, Y. & McCauley, J. GISAID: Global initiative on sharing all influenza data – from vision to reality. *Euro Surveill* **22** (2017). https://doi.org/10.2807/1560-7917.ES.2017.22.13.30494

52 Li, W. & Godzik, A. Cd-hit: a fast program for clustering and comparing large sets of protein or nucleotide sequences. *Bioinformatics* **22**, 1658–1659 (2006). https://doi.org/10.1093/bioinformatics/btl158

53 Krissinel, E. & Henrick, K. Inference of macromolecular assemblies from crystalline state. *J Mol Biol* **372**, 774–797 (2007). https://doi.org/10.1016/j.jmb.2007.05.022

54 Punjani, A., Rubinstein, J. L., Fleet, D. J. & Brubaker, M. A. cryoSPARC: algorithms for rapid unsupervised cryo-EM structure determination. *Nat Methods* **14**, 290–296 (2017). https://doi.org/10.1038/nmeth.4169

55 Sanchez-Garcia, R. *et al.* DeepEMhancer: a deep learning solution for cryo-EM volume post-processing. *Commun Biol* **4**, 874 (2021). https://doi.org/10.1038/s42003-021-02399-1

56 Jamali, K. *et al.* Automated model building and protein identification in cryo-EM maps. *Nature* **628**, 450–457 (2024). https://doi.org/10.1038/s41586-024-07215-4

57 Emsley, P., Lohkamp, B., Scott, W. G. & Cowtan, K. Features and development of Coot. *Acta Crystallogr D Biol Crystallogr* **66**, 486–501 (2010). https://doi.org/10.1107/S0907444910007493

58 Agirre, J. *et al.* Privateer: software for the conformational validation of carbohydrate structures. *Nat Struct Mol Biol* **22**, 833–834 (2015). https://doi.org/10.1038/nsmb.3115

59 Liebschner, D. *et al.* Macromolecular structure determination using X-rays, neutrons and electrons: recent developments in Phenix. *Acta Crystallogr D Struct Biol* **75**, 861–877 (2019). https://doi.org/10.1107/S2059798319011471

60 Williams, C. J. *et al.* MolProbity: More and better reference data for improved all-atom structure validation. *Protein Sci* **27**, 293–315 (2018). https://doi.org/10.1002/pro.3330

61 Crawford, K. H. D. & Bloom, J. D. alignparse: A Python package for parsing complex features from high-throughput long-read sequencing. *J Open Source Softw* **4** (2019). https://doi.org/10.21105/joss.01915

62 Zhang, J., Kobert, K., Flouri, T. & Stamatakis, A. PEAR: a fast and accurate Illumina Paired-End reAd mergeR. *Bioinformatics* **30**, 614–620 (2014). https://doi.org/10.1093/bioinformatics/btt593

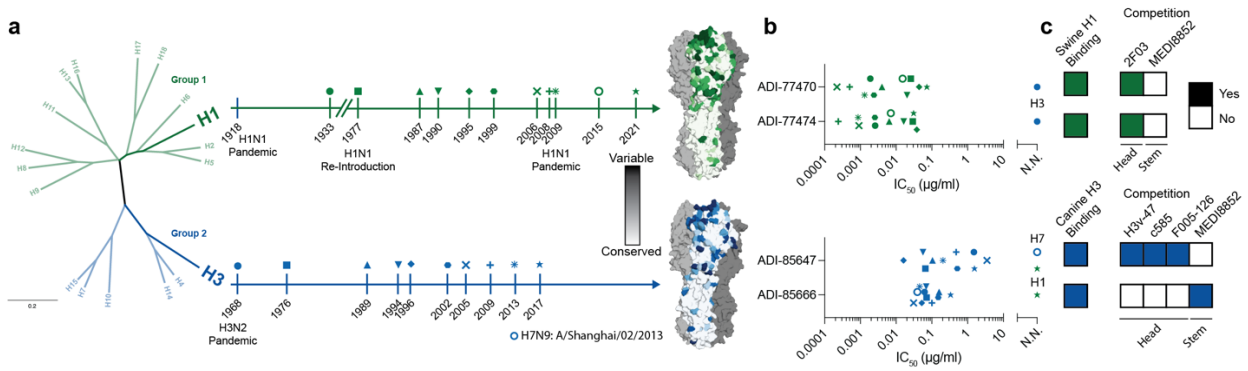

Fig. 1: Broad subtype neutralization by human antibodies targeting the HA head. (**A**) Diversity of influenza A HA. Phylogenetic tree of influenza A virus HAs (left). Timeline of influenza H1N1 and H3N2 circulation; symbols represent strains used in this study (middle). Pairwise identity of HAs from viruses used in this study mapped onto structures of HA (PDB: 3LZG and 4FNK) (right). (**B**) Neutralization potencies determined by microneutralization for down-selected antibodies against a panel of influenza A viruses. Strains are indicated as in **A**. H1N1 strains: A/WSN/1933, A/USSR/90/1977, A/Memphis/4/1987, A/Massachusetts/1/1990, A/Beijing/262/1995, A/New Caledonia/20/1999, A/Solomon Islands/3/2006, A/New York/08-1326/2008, A/California/07/2009, A/Michigan/45/2015, A/Sydney/5/2021. H3N2 strains: A/Aichi/2/1968, A/Bilthoven/1761/1976, A/Beijing/353/1989, A/Johannesburg/33/1994, A/Brisbane/8/1996, A/Fujian/411/2002, A/Wisconsin/67/2005, A/Perth/16/2009, A/Switzerland/9715293/2013, A/Kansas/14/2017. (**C**) ELISA binding reactivity at 10 or 1 µg/ml to A/Swine/Henan/SN13/2018[30] or A/Canine/Hainan/79/2019[31] (left) and BLI-based antibody competition with the indicated antibodies (right).

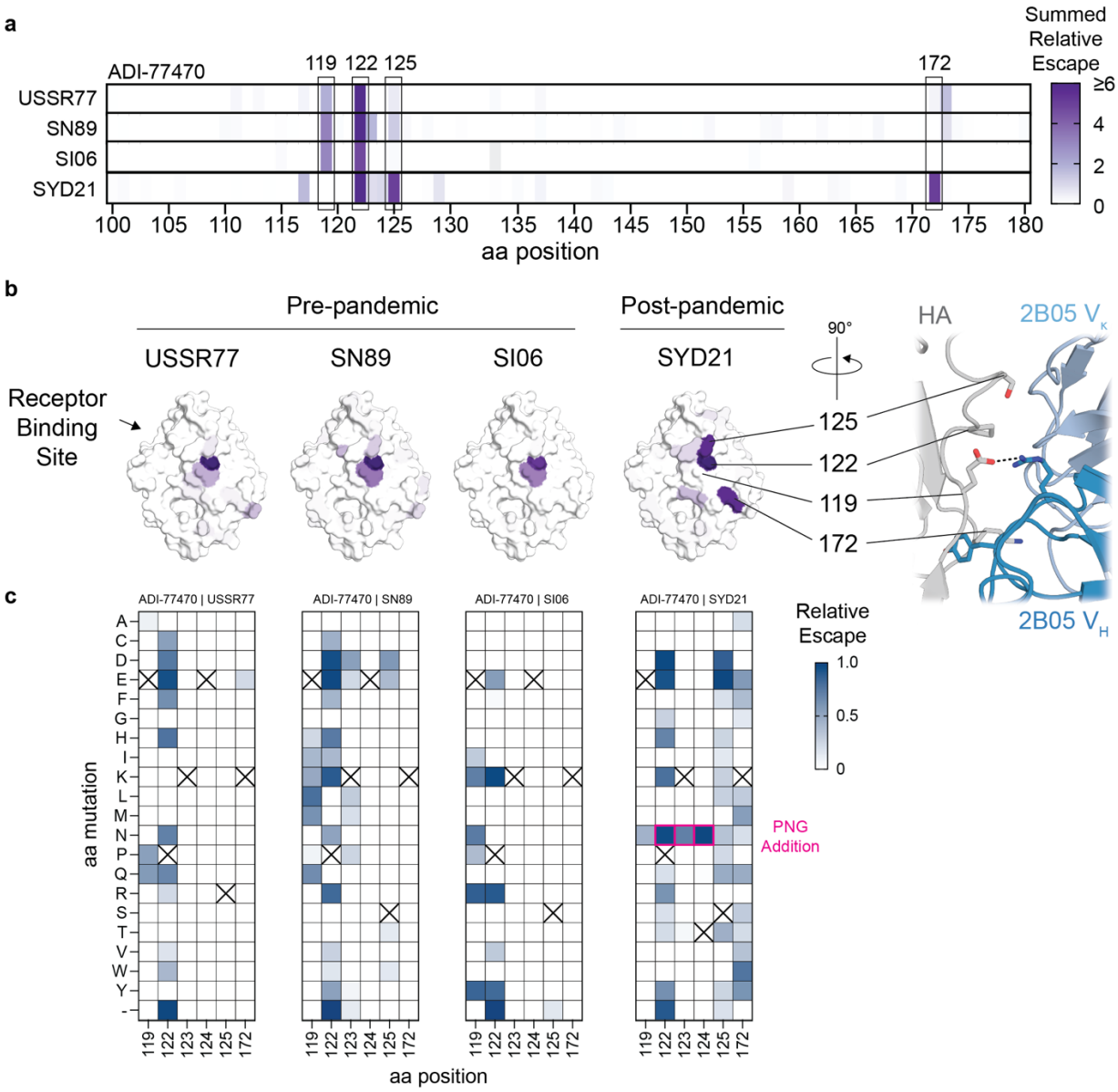

Fig. 2: Escape from a broad H1 neutralizing antibody in multiple H1N1 viruses. (**A**) Relative escape values summed by amino acid position in the HA head (H3 numbering) for ADI-77470 against USSR77 (A/USSR/90/1977), SN89 (A/Siena/10/1989), SI06 (A/Solomon Islands/3/2006), and SYD21 (A/Sydney/5/2021). (**B**) Summed relative escape values shown in **A** mapped onto the structure of the SI06 head (PDB: 4HKX) (left) with specific residues highlighted on the structure of the lateral patch-targeting antibody 045-09 2B05 bound to A/California/04/2009 (PDB: 7MEM) (right). (**C**) Relative escape values from ADI-77470 for individual amino acid mutations for each of the strains in **A** for a subset of positions. Highlighted asparagine mutations in SYD21 add potential N-linked glycosylation (PNG) sites.

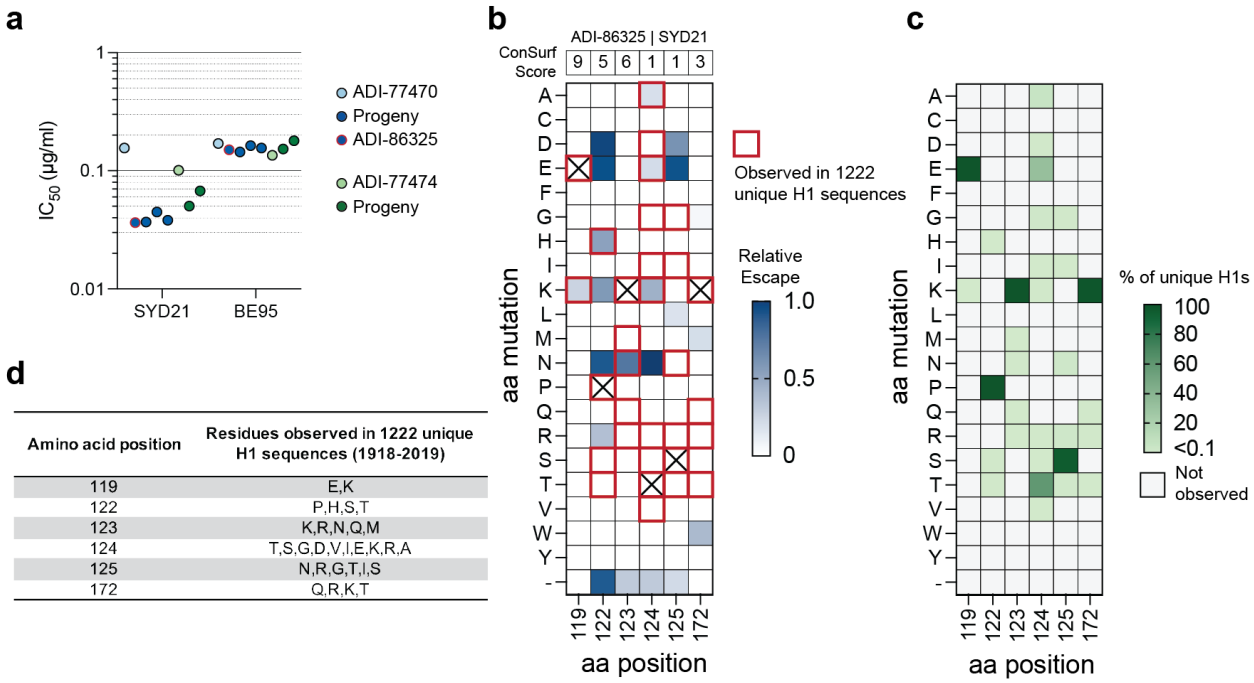

d

Amino acid position	Residues observed in 1222 unique H1 sequences (1918-2019)
119	E,K
122	P,H,S,T
123	K,R,N,Q,M
124	T,S,G,D,V,I,E,K,R,A
125	N,R,G,T,I,S
172	Q,R,K,T

Fig. 3: Naturally occurring escape mutations from an engineered lateral patch antibody are rare. (**A**) Neutralization potencies for in vitro affinity-matured antibodies against SYD21 (A/Sydney/5/2021) and BE95 (A/Beijing/262/1995). (**B**) Relative escape values from ADI-86325 for individual amino acid mutations in SYD21 for the positions that can cause escape. ConSurf[36] values from a previous analysis[35] are shown at the top. Amino acids boxed in red indicate these were observed in the ConSurf analysis of 1222 H1 sequences that are representative of sequence clusters[35]. (**C**) Frequency of observed mutations in the same set of 1222 unique H1 sequences. (**D**) Table of observed residues at each position.

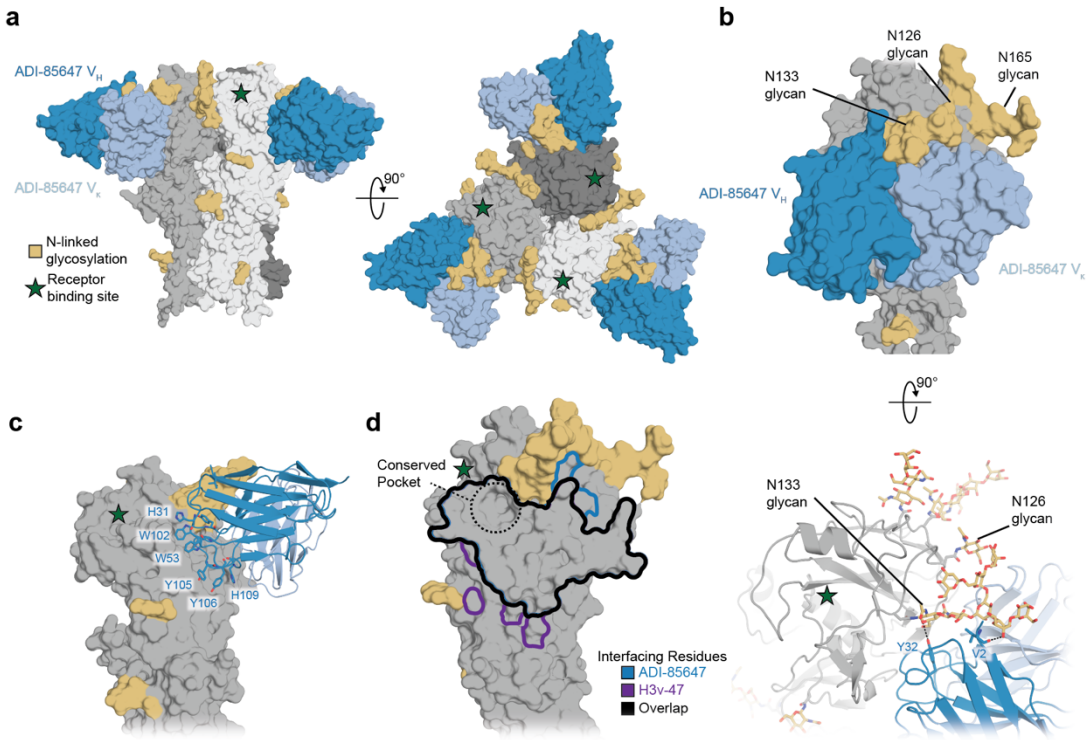

Fig. 4: A broad H3 antibody targeting the side of the HA head. (**A**) Cryo-EM structure of ADI-85647 bound to DAR21 (A/Darwin/6/2021) HA. (**B**) A glycan at N133 sits within a cleft formed between the V_H and V_κ of ADI-85647 (top). Hydrogen bonds formed between the N133 glycan and the V_H of ADI-85647 (bottom). (**C**) Several aromatic residues in the heavy chain interact with DAR21 HA. (**D**) The epitopes of ADI-85647 and H3v-47 are highlighted, showing the high degree of overlap between the two epitopes. PISA[53] was used to determine interfacing residues.

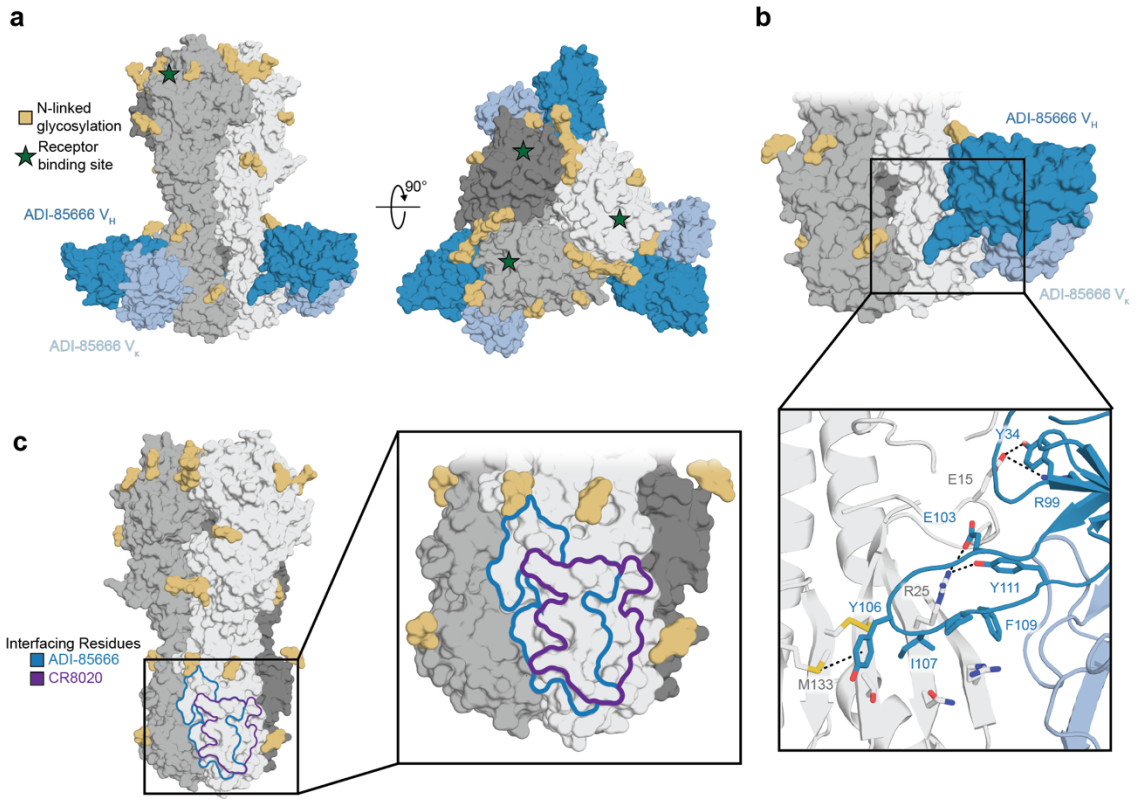

Fig. 5: A group 2 neutralizing antibody targets a unique epitope in the stem. (**A**) Cryo-EM structure of ADI-85666 bound to DAR21 (A/Darwin/6/2021) HA. (**B**) Close up of the interactions between the CDRH3 of ADI-85666 and DAR21 HA. (**C**) The epitopes of ADI-85666 and CR8020 are highlighted showing overlapping, but distinct epitopes. PISA[53] was used to determine interface residues.

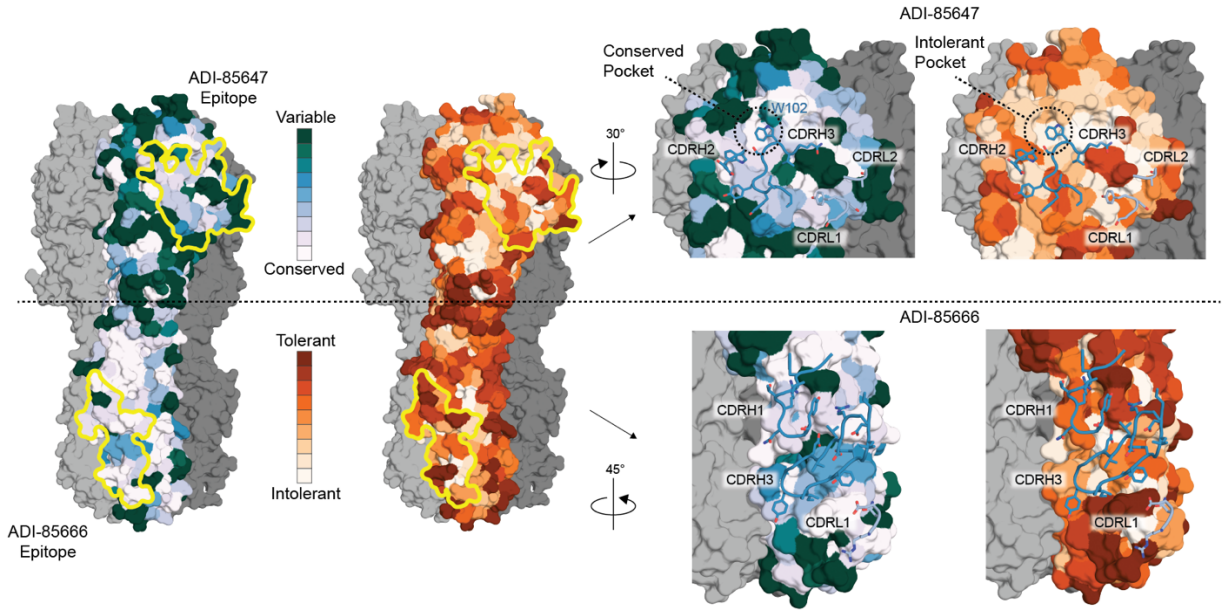

Fig. 6: Conservation of epitopes targeted by broad H3 antibodies. ConSurf[36] scores from 3408 unique H3 HA sequences and mutational tolerance values (0.3-2.7)[28] are mapped onto the cryo-EM structure of A/Darwin/6/2021 HA. Footprints of ADI-85647 and ADI-85666 are outlined (left). CDRs from ADI-85647 (top, right) and ADI-85666 (bottom, right) are shown in the context of the ConSurf scores and mutational tolerance values. Color spectrums were obtained from colorbrewer2.org.